Acta Materialia 271 (2024) 119869

Contents lists available at ScienceDirect

Acta Materialia

journal homepage: www.elsevier.com/locate/actamat

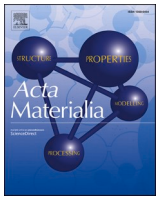

Full length article

Dual-layer FePt-C granular media for multi-level heat-assisted magnetic recording

P. Tozman [a,*], S. Isogami [a], I. Suzuki [a], A. Bolyachkin [a], H. Sepehri-Amin [a], S.J. Greaves [b], H. Suto [a], Y. Sasaki [a], T.Y. Chang [c], Y. Kubota [c], P. Steiner [c], P.W. Huang [c], K. Hono [a], Y.K. Takahashi [a,*]

[a] National Institute for Materials Science, Tsukuba, Ibaraki 305-0047, Japan
[b] Research Institute of Electrical Communications Tohoku University, Sendai, Japan
[c] Seagate Technology, Recording Media Organization, Fremont, CA 94538, United States

ARTICLE INFO

Keywords:
Magnetic recording medium
Multilevel recording
HAMR
Advanced characterization
FePt dual layers
Micromagnetic simulation
Read/write simulation
Magnetic measurement

ABSTRACT

Multi-level magnetic recording is a new concept for increasing the data storage capacity of hard disk drives. However, its implementation has been limited by a lack of suitable media capable of storing information at multiple levels. Herein, we overcome this problem by developing dual FePt-C nanogranular films separated by a Ru-C breaking layer with a cubic crystal structure. The FePt grains in the bottom and top layers of the developed media exhibited different effective magnetocrystalline anisotropies and Curie temperatures. The former is realized by different degrees of ordering in the $L1_0$-FePt grains, whereas the latter was attributed to the diffusion of Ru, thereby enabling separate magnetic recording on each layer under different magnetic fields and temperatures. Furthermore, magnetic measurements and heat-assisted magnetic recording simulations showed that these media enabled 3-level recording and could potentially be extended to 4-level recording, as the ↑↓ and ↓↑ states exhibited non-zero magnetization.

1. Evolution of magnetic recording

The digital transformation from Industry 4.0 to 5.0 has resulted in significant growth in big data, increasing the demand for data storage [1–3]. However, with the expected increase in energy consumption owing to the construction of more data centers, an environmentally friendly solution is required to satisfy this demand. One solution involves increasing the storage capacity of hard disk drives (HDDs), which currently serve as the primary storage devices in data centers. HDDs comprise a spinning disk coated with a nanogranular ferromagnetic layer (media) and read/write head that magnetically reads and writes data to the disk. The storage capacity of HDDs is determined by the bit size, which refers to the physical dimensions of the region on the media where several ferromagnetic nanograins are magnetized in the same direction. Reducing the bit size facilitates increased data storage in the same physical space [4], thereby increasing the areal density of data bits from the current value of 1.5 Tbit/in^2 to 4 Tbit/in^2 and beyond [3–8]. This is achieved by reducing the grain size of the granular media while maintaining the long-term thermal stability of the data by satisfying the condition $K_uV/k_BT > 60$, where K_u is the uniaxial magnetocrystalline anisotropy constant, V is the volume of a grain, k_B is the Boltzmann constant, and T is the temperature [9,10]. This condition is fulfilled by $L1_0$-FePt granular media, where FePt grains with a very high K_u ≈7 MJ/m^3 are uniformly dispersed in a nonmagnetic segregant [7,9,11,12]. However, this medium cannot be used in conventional recording technologies because it requires a high magnetic field, more than 3 T, for the writing process. This problem is overcome via heat-assisted magnetic recording (HAMR), which facilitates the writing of data on high-K_u and high-coercivity (H_c) media materials [11,13]. Unlike conventional recording, HAMR equips a write head with a near-field transducer (NFT) to heat a small area on the recording media around its Curie temperature T_c, thereby lowering the high-K_u locally and enabling the switching of the magnetization direction by a write field generated from the write head (Fig. 1(a)). The grains are heated as a result of the internal current generated within the grains themselves, induced by the localized electric field produced by the NFT which is located near to the grains.

According to the Advanced Storage Research Consortium (ASRC), the primary focus for increasing the areal density in HAMR is to improve

* Corresponding authors.
E-mail addresses: pelin.tozman@tu-darmstadt.de (P. Tozman), takahashi.yukiko@nims.go.jp (Y.K. Takahashi).

https://doi.org/10.1016/j.actamat.2024.119869
Received 5 October 2023; Received in revised form 2 February 2024; Accepted 23 March 2024
Available online 24 March 2024

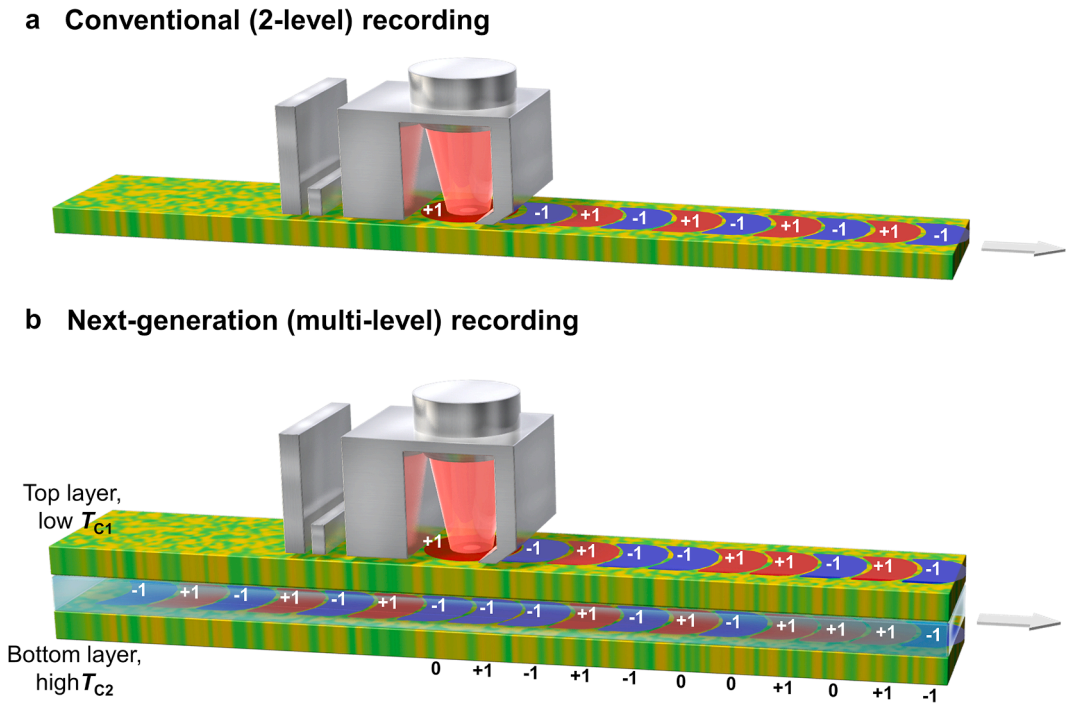

Fig. 1. Schematic of the concept of multi-level magnetic recording compared to current 2-level magnetic recording technology in hard disk drives. In both cases, a small area on the recording medium is heated to approximately its T_c to switch the magnetization. The arrow indicates the writing direction. An optical transducer provides a Gaussian heat spot (red color) utilized to heat the area. The magnetic state is stored by cooling the heated area to ambient temperature. (a) In the conventional 2-level recording, the laser power is set as a constant, and magnetization switches by changing the polarity of the write field to obtain a magnetization pattern with (↑ ("1″) and ↓("−1")). (b) For multi-level recording, the laser power is tuned along with the polarity of the write field to manipulate the magnetization switching of each layer. During the first write operation, a high laser power is set to heat a small area above T_{c2} of the bottom layer ($T>T_{c2}$) and thus write both layers. During the second write, the laser power is lowered below T_{c2} ($T>T_{c1}$) to write only the top layer. This delivers four different magnetic states (↑↑ ("1″), ↓↓ ("−1"), ↑↓ ("0″), and ↓↑ ("0")) which correspond to a 4-level recording. The recording medium is only a few nm thick, while the breaking layer is half that thickness.

the nanostructure of the granular FePt-X media [7,9], where X indicates nonmagnetic segregants. By refining the grain size to 4.3 nm and obtaining a high degree of $L1_0$-order, the areal density is expected to reach 4 Tbit/in^2 [7,9,10,14,15]. To achieve such a fine microstructure, various X, including metal oxides, B, h-BN, B_4C, and C, have been added to FePt-based granular films, with C and h-BN providing a small average grain size, $<D>$= 5–8 nm while maintaining uniaxial anisotropy [11, 14-20]. Thus, a maximum areal density of 2.77 Tbit/in^2 was achieved by Seagate for a demo HAMR [3].

However, FePt grains smaller than 4 nm ($<D> < 4$ nm) cannot maintain their crystallographic $L1_0$ order, resulting in thermal fluctuations of the magnetization owing to the low anisotropy energy [18]. Therefore, increasing the areal density of future generations of HDD recording media requires a new recording concept that is not reliant on grain size miniaturization [8,21]. One solution is bit-patterned media (1 bit = 1 grain) instead of granular media (1 bit = multiple grains). Numerical calculations predicted that bit-patterned media can achieve an areal density of 10 Tbit/in^2 [21–23]. However, bit-patterned media cannot be mass produced because of their costly nanofabrication process. Another solution involves the use of multi-level recording [24–26], as explained in the following Section.

2. Concept of multi-level recording in HAMR

A multi-level recording concept has been proposed for HAMR technologies, which uses media comprising multiple recording layers with different T_c and controls the magnetization reversal in each layer by tuning the temperature of the heated spot [27–29]. Fig. 1 shows a schematic of the dual-layer version of a multi-level HAMR in comparison with the traditional single-layer version of a 2-level HAMR. The single-layer version employs a constant laser power to heat a small region of the magnetic layer around T_c, and the write field is used to switch the magnetization direction between the up ↑ ("1″) and down ↓ ("−1") magnetization states. This facilitates the storage of a single bit of data (Fig 1(a)) [7,13]. Following the magnetization switch, the heated region is rapidly cooled under an applied field to store the magnetic polarity of the region.

It should be noted that even in a single layer of sufficient thickness, it may be possible to realize multiple magnetization states with one-pass recording via random pinning of a reverse domain due to thermal fluctuations during the cooling of the FePt grains [30]. However, in the dual-layer version, multi-level recording is achieved through a two-pass recording process, wherein the Curie temperature of the bottom layer, T_{c2}, is higher than that of the top layer T_{c1} ($T_{c1} < T_{c2}$) [29,31]. This version assumes a 1:1 grain growth correlation between the top and bottom layers. The layers are separated by a thin, metallic granular exchange-breaking layer, facilitating efficient heat conduction from the top layer to the bottom layer. In the first write, the laser power is high to align the magnetization direction of the bottom layer with the polarity of the write field. Moreover, during the first write, the top layer is inevitably also written because of its low T_c, resulting in the same magnetization pattern being written to both layers, i.e. the up ↑↑ ("1″) and down ↓↓ ("−1") magnetization states, similar to single-layer HAMR. Thereafter, in the second write, the laser power is lowered to facilitate writing in only the upper layer without disturbing the magnetization configuration of the bottom layer. This process produces four magnetic states corresponding to ↑↑ ("1″), ↓↓ ("−1"), ↑↓ ("0″), and ↓↑ ("0"), as shown in Fig. 1(b). These additional magnetization states extend the recording from the conventional 2-levels to 3-levels, and can potentially be extended to 4-levels if the read head can distinguish between the ↑↓ and ↓↑ states.

Experimentally, T_{c1} can be differentiated from T_{c2} either by varying

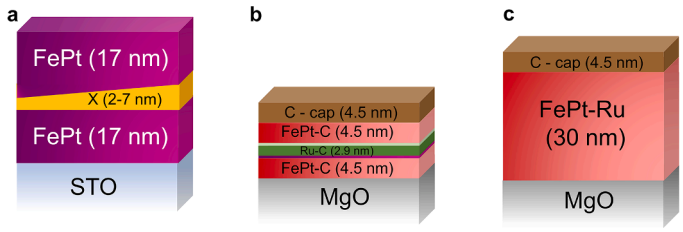

Fig. 2. Schematic representation of film structures for (a) STO / $Fe_{50}Pt_{50}$ (17 nm) / X (2–7 nm) / $Fe_{50}Pt_{50}$ (17 nm) for X = Ru, Cu, and Pt (b) MgO / $Fe_{51}Pt_{49}$–C (20 vol.%) (4.5 nm) / $Fe_{51}Pt_{49}$ (0.26 nm) /Ru-C (20 vol.%) (2.9 nm) / Ru (0.11 nm) / $Fe_{51}Pt_{49}$–C (20 vol.%) (4.5 nm) / C where pink indicates the thin FePt layer and light green indicates the thin Ru layer (c) MgO / FePt-Ru (30 nm) / C (4.5 nm) where $Fe_{42}(Pt_{58-x}Ru_x)$ for x = 0, 0.5, 2, 4 and 8 at.%.

the Fe content in FePt or by using various additives in FePt, such as Cu, Ni, Cr, Mn, B, and Ag [11,12,15,17,29,32-35]. These layers can be magnetically decoupled by introducing a breaking layer between them. In this study, we developed the first experimental synthesis of a multi-level recording medium. Its nanostructure, magnetization-switching mechanism, and read/write performance were investigated using experimental and numerical tools.

3. Experimental techniques

All the films were prepared using an ultrahigh-vacuum co-sputtering system with a base pressure of approximately 10^{-7} Pa (Fig. 2). To investigate the breaking layer, FePt (17 nm)/X (with a gradual thickness (2–7 nm)/ FePt (17 nm)) was deposited on an STO (001) substrate at 500 °C for X = Ru, Cu, and Pt. These film stacks were grown using a $Fe_{50}Pt_{50}$ target. The dual-layer films were patterned into Hall bars for transverse Hall bar resistance measurements. An alternating MgO/ $Fe_{51}Pt_{49}$–C film stack (20 vol.%) (4.5 nm)/ $Fe_{51}Pt_{49}$ (0.26 nm)/Ru-C (20 vol.%) (2.9 nm)/Ru (0.11 nm)/ $Fe_{51}Pt_{49}$–C (20 vol.%) (4.5 nm)/C-cap was grown at 500 °C as a granular, dual layer medium. The average heights of the layers (FePt-C (5.5 ± 0.7 nm)/Ru-C (3.0 ± 0.6 nm)/ FePt-C (5.1 ± 0.6 nm)/) obtained from the EDS maps were consistent with the design. Thin FePt and Ru layers were deposited to prevent C migration. A C capping layer was deposited at 300 K to prevent surface oxidation. MgO single-crystal substrates are preferred for promoting a strong [001] texture and minimizing misorientation in (001)-textured FePt grains [9, 36]. The film stack of MgO/FePt-Ru (30 nm)/C-cap (4.5 nm) with the composition of $Fe_{42}(Pt_{58-x}Ru_x)$ for x = 0, 0.5, 2, 4 and 8 at.% was grown at a substrate temperature of 500 °C to perform the comparisons. All film stacks were grown by co-sputtering FePt targets with the composition of $Fe_{51}Pt_{49}$ with Ru or C targets.

X-ray diffraction (XRD) Rigaku SmartLab with a Cu X-ray source was used for crystallographic and degree of $L1_0$ order analyses. Electron-transparent thin specimens were prepared for transmission electron microscopy (TEM) using a focused ion beam lift-out technique (FEI Helios Nanolab 650). To prevent damage during the ion beam milling, the film surfaces were coated with Ni. TEM was performed using a Titan G2 80–200 with a probe aberration corrector. Energy-dispersive X-ray spectroscopy (EDS) was conducted using an FEI Super-X EDX detector. A 7 T Quantum Design superconducting quantum interference device magnetometer (SQUID) was used for the magnetic measurements. The films were embedded in high-temperature cement for the measurements at temperatures above 380 K. The Curie temperature (T_c) was determined by the least squares fitting using Kuz'min's equation [37]. The magnetization direction (θ_M) dependences of torques were measured using the anomalous Hall effect to deduce the first- and second-order uniaxial anisotropy constants K_1 and K_2 as described by Ono et al. [38].

4. Micromagnetic approximation of hysteresis loops

A finite element model of a dual-layer FePt granular medium was developed using Voronoi-based tessellation. The bottom layer was represented by 5 nm thick columnar grains with a top-view grain size of 12.5 (2.0) nm, which reproduced the experimental grain size

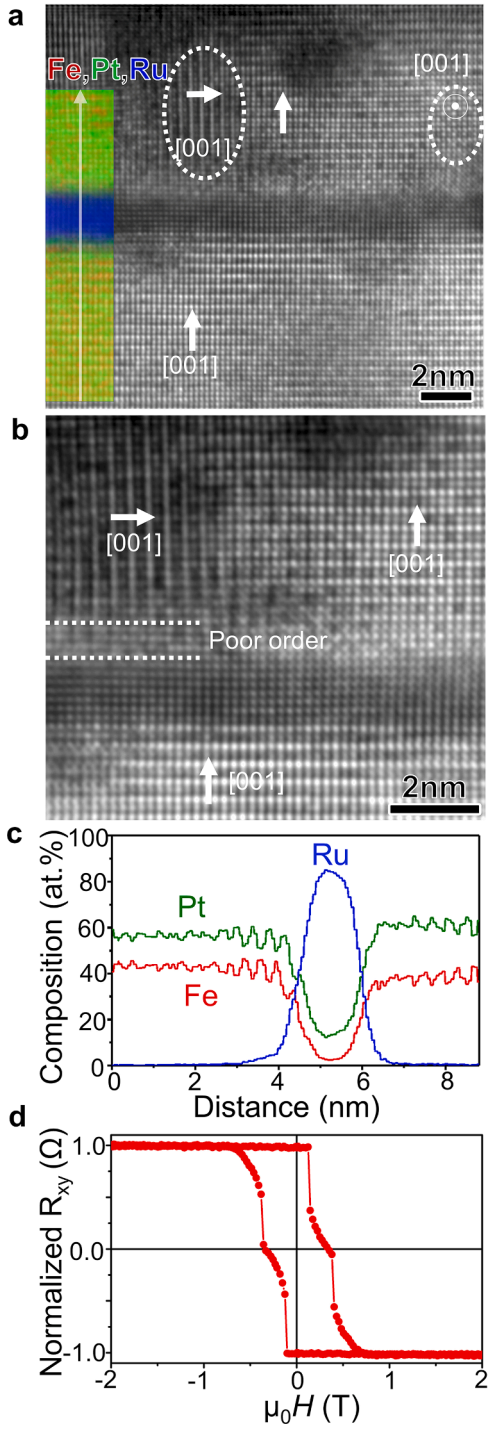

Fig. 3. Microstructural features of FePt/Ru/FePt continuous film. (a, b) HAADF and STEM-EDS maps of Fe, Pt, and Ru with (c) line scan for FePt (17 nm)/Ru (2 nm)/FePt (17 nm). **c** EDS line scan reveals the difference in the composition of the top and bottom layers, with a trace amount of Ru diffusion into the bottom. (d) Transverse normalized Hall-bar resistance (R_{xy}) measurement as a function of the external magnetic field, where R_{xy} corresponds to the out-of-plane of the magnetization, showing that each layer has a different switching field.

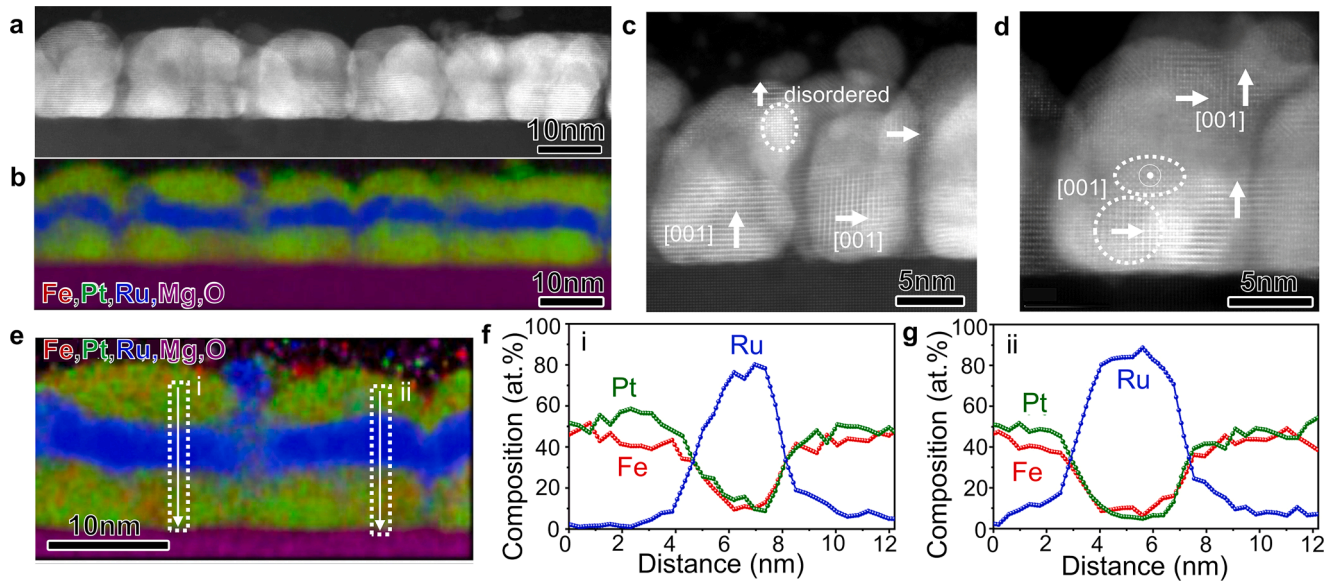

Fig. 4. Overall nanostructure of the developed media for multi-level magnetic recording is shown in (a) HADDF image (b) EDS map for FePt-20 vol.% C/Ru- 20 vol% C/FePt-20 vol% C of granular dual layer media shows that FePt-C layers are separated by using a Ru-C breaking layer. (c, d) High magnification HADDF images indicate that the additional in-plane variants are present on the top layer, in addition to the (001) texture. (e) High magnification EDS map with (f, g) its line scan revealing that Ru diffuses to both the layers and the intergranular region.

distribution. The top layer with a thickness of t_{top} was fabricated by the out-of-plane translation of the bottom layer through a 3-nm-thick nonmagnetic gap (breaking layer). Following the TEM observations of the real samples, in-plane variants were introduced into the model by randomly splitting certain grains into several regions with mutually orthogonal easy magnetization axes. The total volume fractions of the in-plane variants were controlled in both layers using V_{top} and V_{bot}. The magnetic anisotropy constant was prescribed to the grains following different distributions with K_{top} and K_{bot} mean values for the top and bottom layers, respectively. Note that for each individual grain, the same anisotropy constant was considered in all the variants that it comprised. The saturation magnetization and exchange stiffness values were assumed to be the same for all grains, that is, $\mu_0 M_s = 1.43$ T and $A = 10$ pJ/m, respectively [39]. Micromagnetic simulations were performed using the FastMag software by solving the Landau–Lifshitz–Gilbert equation with a damping constant $\alpha = 1$ [40]. The parameters t_{top}, V_{top}, K_{top}, V_{bot}, and K_{bot} were varied in a grid-search manner to approximate the experimental hysteresis loops.

5. Multilevel HAMR recording simulation

The model used the Landau–Lifshitz–Bloch equation, which is suitable for modeling the behavior of magnetic materials at temperatures up to and beyond T_c [41]. The temperature dependence of M_s was calculated by assuming a Brillouin function with $J = 1$, and K_u was derived from M_s as $K_u(T) \sim M_s(T)^2$ [42]. Each image depicts the average magnetization of 50 tracks, where a magnetic head was used to read or write data. The simulation parameters used were the experimental T_c and predicted K_u based on the experimental *M-H* loops. The recording medium had an average grain size, average grain pitch, and grain size distribution of 13 nm, 14 nm, and 19%, respectively. The top and bottom layers were both 6 nm thick, separated by a 3 nm nonmagnetic layer. The heat spot was moved along the medium at a velocity of 4 m/s. The ambient temperature was set at 300 K. The heat spot had a two-dimensional Gaussian temperature distribution in the media, with a half width at half maximum (HWHM) of 50 nm, i.e. the temperature at 50 nm distance from the center of the heat spot was $300 + [0.5 \times (T_{max} - 300)]$ K, where T_{max} was the maximum temperature.

6. Results and discussions

6.1. Breaking layer

We experimentally investigated various nonmagnetic metallic breaking layers (BL) to magnetically decouple the top and bottom recording layers to realize multi-level recording. An ideal BL should facilitate the growth of the top FePt layer with a smooth and flat surface, high K_u, and (001) epitaxy. To select the most appropriate BL, we first modeled the idealized interface between the FePt layers using a continuous film, not a granular one. Consequently, the effects of mismatch strain and surface roughness were minimized, and only the effect of the BL on the magnetic properties, particularly on the switching separation, was investigated. Ru, Cu, Pt, and W were considered for use as a BL owing to their small lattice mismatch (0.5–1.7%) with FePt (Supplementary Fig. S1). High-magnification, cross-sectional high-angle annular dark field (HAADF) and scanning transmission electron microscopy (STEM) images showed that, among these elements, only Ru and Pt exhibited a flat interface with (001) epitaxial growth (Fig. 3 (a,b) and Supplementary Fig. S2). Currently, Pt is not considered because both layers exhibit the same composition, resulting in similar T_{c1} and T_{c2} values in their *M-T* curves. In contrast, compositional differentiation occurs in the case of face-centered cubic (fcc) Ru [43]. The energy-dispersive X-ray spectroscopy (EDS) line scan profile shows the difference in the composition of the top ($Fe_{39}Pt_{61}$) and bottom ($Fe_{42}Pt_{58}$) layers and the diffusion of trace amounts into the bottom within a depth of approximately 1 nm from the Ru layer (Fig. 3(a,c)). This is expected to induce a difference in the T_c values, which is essential for multi-level recording [44]. In addition, despite the predominant (001) epitaxy, the top FePt layer also displayed in-plane variants and a lack of $L1_0$ order during the initial stage of growth (~1 nm) (Fig. 3(a,b)). This affects the effective anisotropy, thus varying the switching field and resulting in a step-like behavior in the Hall bar resistance measurement corresponding to the two coercivity values (Fig. 3(d)). The W and Cu breaking layers formed unexpected (111) epitaxies and island-like microstructures, respectively, as shown in Supplementary Fig. S3.

Although Ru magnetically decoupled the top and bottom layers, it diffused locally into the bottom layer and created local variants and disordered regions in the top layer. Therefore, to understand the

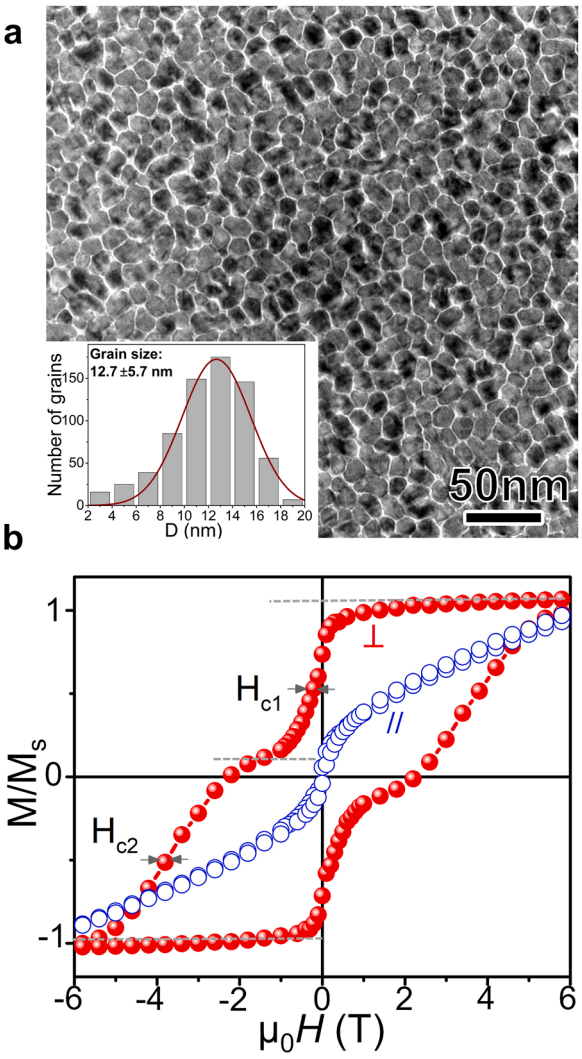

Fig. 5. Microstructure of granular FePt-C/Ru-C/FePt-C films and corresponding magnetization curves. (a) In-plane bright-field TEM images, with an inset showing the grain size distribution, reveal that the average grain size is 12.7± 5.7 nm. (b) Corresponding out-of-plane (⊥) and in-plane (//) magnetization curves show that $\mu_0 H_{c1}$= 0.24 T and $\mu_0 H_{c2}$ = 3.82 T.

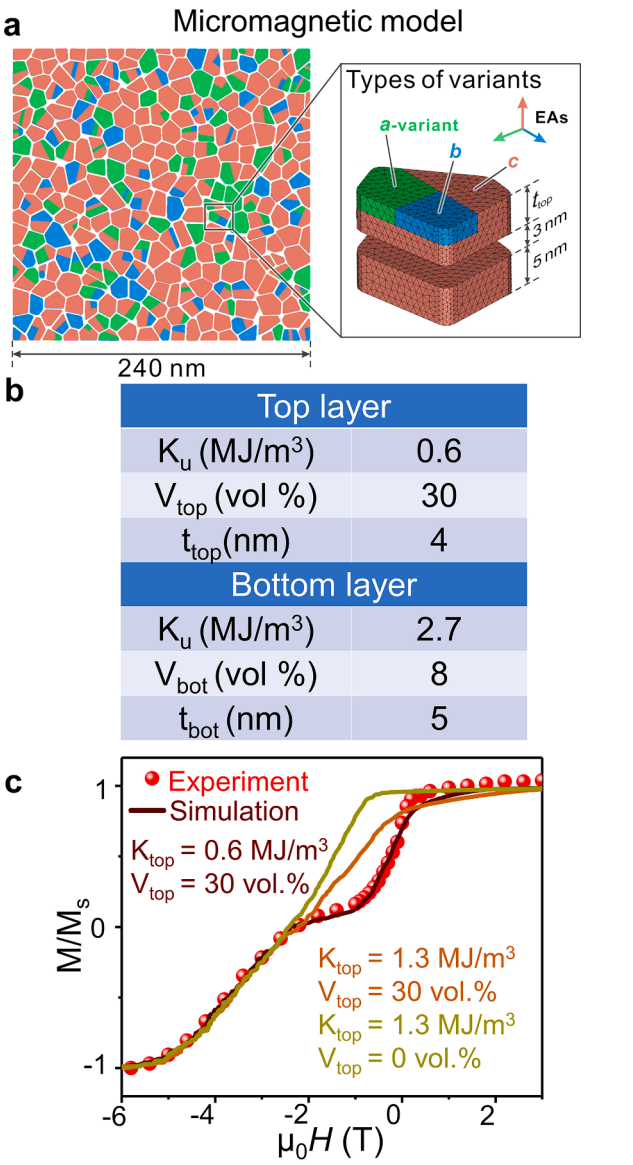

Fig. 6. (a) Top view of the micromagnetic model of dual-layer FePt media with an enlarged grain showing in 3D the splitting of the top layer into in-plane variants (*a* and *b* variants). (b) Estimated parameters for the FePt-C/Ru- C/FePt with 20% vol. of C in each layer, that is, mean magnetic anisotropy constant (K_u) and its standard deviation, the volume fraction of the in-plane variants (V), and layer thickness (t). (c) The simulated (line) and experimental (dots) *M-H* curves are shown together. Besides the best approximation of the experimental data, simulated curves (displayed with orange and green color) also show potential *M-H* curves if K_{top} and V_{top} are improved.

comprehensive effect of Ru on the magnetic properties and chemical order, a continuous FePt layer was grown on MgO substrates with Ru contents of $x = 0$, 0.5, 2, 4, and 8 at.%. Ru substitution decreased the $L1_0$ order while increasing the lattice parameter c (Supplementary Fig S4). Therefore, one reason for the partially disordered region could be the diffusion of Ru into the FePt layers, which results in a different strain state owing to the expansion of the lattice parameter.

The effective anisotropy constant of K_u for $x = 0$ in $Fe_{42}Pt_{58}$ was 3.06 MJ/m^3 at 300 K, which is consistent with the literature [45]. Increasing the Ru content to $x = 8$ in $Fe_{42}(Pt_{58-x}Ru_x)$ decreased K_u to 0.8 MJ/m^3 (Supplementary Fig. S5) [35]. Therefore, K_u as well as H_c, can be modified in each layer via Ru substitution or diffusion. Further, T_c decreased from 610 K for $Fe_{42}Pt_{58}$ to 540 K via the substitution of a small amount of Ru in $Fe_{42}Pt_{57.5}Ru_{0.5}$ (Supplementary Fig. S6 (a,b)) [35,44,46]. The modification of K_u and T_c via Ru introduction benefits multi-level recording by controlling the magnetization reversal in each layer if the Ru substitution remains at $x \leq 0.5$ at.%.

6.2. Dual nanogranular magnetic layers

Dual nanogranular magnetic layers as a multi-level recording medium was obtained by growing a (001)-textured FePt-20 vol.% C granular bottom layer (4.5 nm) on a MgO (001) substrate, followed by a Ru-C breaking layer (2.9 nm) and FePt-C granular top layer. This was confirmed via the cross-sectional HAADF-STEM image and EDS map in Fig. 4 (a,b). Carbon is preferred as a segregant to reduce the average grain size and maximize the grain density while maintaining the $L1_0$ order [14,39,47]. The FePt grains primarily exhibited a columnar shape with a relatively flat surface and certain curved grains. In Fig. 4(c), the high-magnification HADDF image reveals that the FePt grains in the bottom layer exhibit mainly well $L1_0$-ordered (001) texture with some in-plane variants. In contrast, the FePt grains in the top layer exhibit more in-plane variants and partially disordered regions. The EDS maps and line scans in Fig. 4(e-g) show that Ru diffused to both layers and to the intergranular region. To investigate the influence of the Ru-C BL on

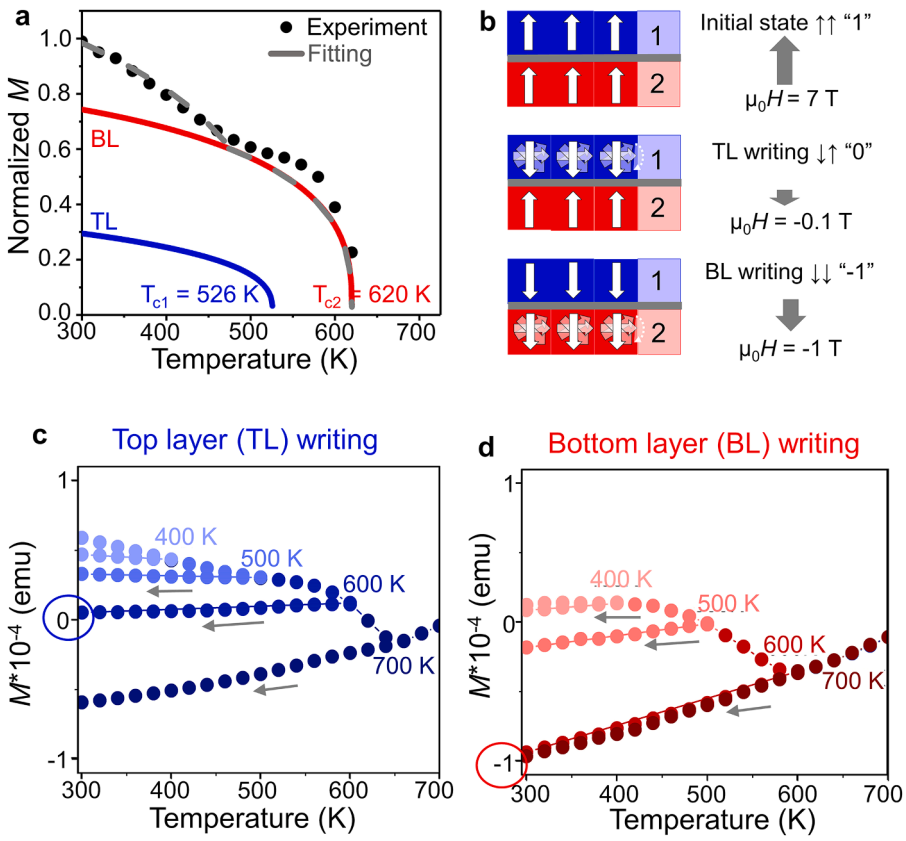

Fig. 7. Temperature-dependent magnetic measurement of granular FePt-C/Ru-C/FePt-C media. (a) *M-T* measurement is performed under 0.1 T wherein the top and bottom layers exhibit T_{c1} of 526 K and T_{c2} of 620 K. (b) Schematic representation of magnetic measurement to mimic the writing procedure. (c) *M-T* measurement under an applied field of μ_0H = - 0.1 T to switch the magnetization of the top layer at 600 K corresponding to the ↓↑ state ("0"). **(d)** Increasing $\mu_0H = -1$ T to switch the magnetization of the bottom layer corresponding to ↓↓ ("−1").

the degree of the $L1_0$ order, the XRD patterns of the single- and dual-layer media were evaluated. The large chemical order parameter, $S = 0.8$, of the single FePt-C layer decreased to 0.63 with the growth of the BL and top layer (Supplementary Fig. S7). Another factor that disturbed the (001) texture was the shape of FePt grains. Interfacial strain is required to suppress the formation of in-plane variants, as is the case for the FePt/MgO interface in the bottom layer [36,48]. However, such strain may lack at the curved Ru-FePt interface, leading to an increase in the number of in-plane variants in the top layer.

The average grain size of the media was obtained as 12.7± 5.7 nm from the top-view bright-field transmission electron microscopy (TEM) images in Fig. 5(a). Fig. 5(b) shows the experimental out-of-plane (OOP) and in-plane (IP) magnetization curves, along with the simulated curves. The IP curve indicates strong perpendicular magnetic anisotropy. Based on half of the mid-distance between the saturation and plateau regions of the OOP curve, the coercivities of the top (H_{c1}) and bottom (H_{c2}) layers were determined to be $\mu_0H_{c1} = 0.24$ T and $\mu_0H_{c2} = 3.82$ T. The large μ_0H_{c2} value confirms good epitaxial growth of the highly ordered FePt (001).

To interpret the magnetic properties of the obtained dual-layer FePt films and distinguish them from the individual layers, the OOP hysteresis loops measured at room temperature were analyzed using micromagnetic simulations (Fig. 6(a)). We reproduced the microstructural features of the films using a finite element model to perform micromagnetic approximations of the demagnetization curves, where the mean magnetic anisotropy constants (K_{top} and K_{bot}), their standard deviations, and the volume fractions of the in-plane variants (V_{top} and V_{bot}) were used as approximation parameters. The table in Fig. 6(b) shows these parameters after such approximation for the FePt-C/Ru-C/FePt-C film with 20 vol.% of C in each layer, i.e., K_{top} and K_{bot} were 0.6 and 2.70 MJ/m^3, while V_{top} and V_{bot} were 30 and 8 vol.%, respectively. Fig. 5(c) shows a nice agreement between the experimental *M-H* curve and one simulated with listed parameters. The increased V_{top} was consistent with the high number of in-plane variants in the top layer observed by high-resolution cross-sectional TEM. The decreased K_{top} was attributed to the deteriorated $L1_0$ order and Ru diffusion (Fig. 4(c)). Both factors contribute to the plateau region in the *M-H* curve. If the in-plane variants are eliminated and K_{top} is improved up to 1.3 MJ/m^3, which is still twice smaller than K_{bot} to distinct switching conditions of the layers, remanence (μ_0M_r) can be restored while the magnetization plateau disappears (Fig. 6(c)). Nevertheless, the high slope d*M*/d*H* still indicates a dual-layer recording system with distinct K_u of the top and bottom layers.

6.3. *Temperature-dependent magnetic measurement and writing simulation*

The T_c of each layer in the dual nanogranular magnetic layers was estimated from *M-T* measurement at 0.1 T in Fig. 7(a), and was found to be $T_{c1} = 526$ K and $T_{c2} = 620$ K. T_c can be affected by various factors such as Ru diffusion, deviation of the Fe and Pt content of the FePt grains, and the $L1_0$ order parameter. Therefore, $T_{c1} = 526$ K may belong to the top layer, which contains most of these factors.

The writing performance of the HAMR media was investigated using temperature-dependent magnetic measurements (Fig. 7(b)). Unlike in the HAMR writing procedure, in this magnetic writing test, the medium was heated as a whole, rather than locally. First, the medium was saturated, corresponding to the magnetic state of ↑↑ ("1″), under 7 T at 300 K. To switch the top layer with a low K_{top} (0.6 MJ/m^3) and T_{c1} (526 K), a small reverse field ($\mu_0H = -0.1$ T) was applied while increasing the

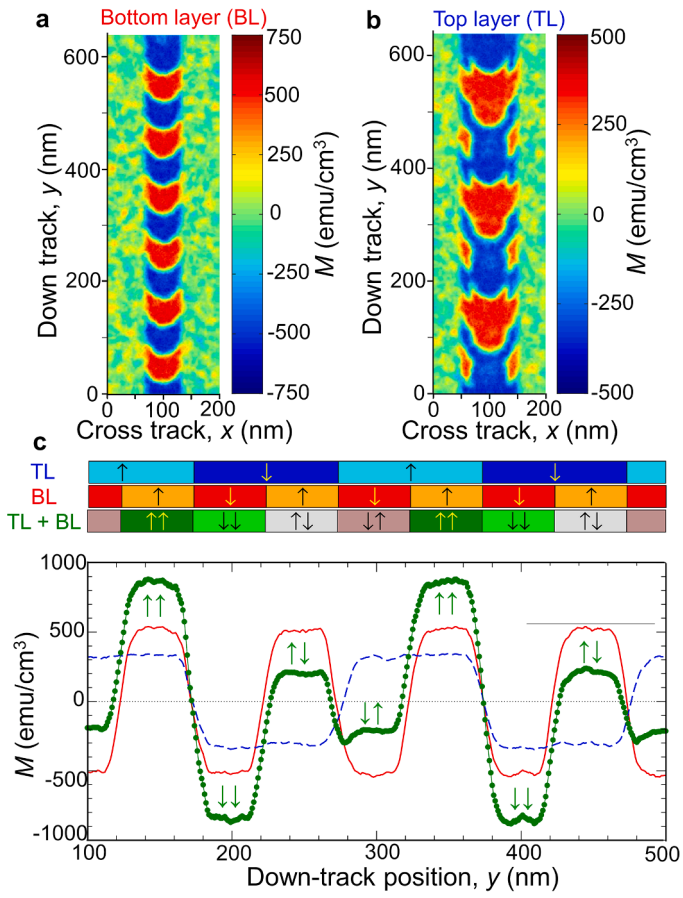

Fig. 8. Multi-level HAMR recording simulation for granular FePt-C/Ru-C/FePt-C media showing the average magnetization patterns of 50 tracks after a two-pass write. (a) Pass 1: Writing on the bottom layer with T_{max} = 680 K, bit length = 50 nm. (b) Pass 2: Writing on the top layer with T_{max} = 540 K, bit length = 100 nm (c) Average magnetization along the down-track direction for the top and bottom layers. The magnetization of the top and bottom layers and the sum of the magnetization of both layers are indicated by the blue dash line, red solid line, and green circles, respectively.

temperature from 300 K to T_{an} = 400, 500, 600, and 700 K. The medium was then cooled to 300 K to store the obtained magnetic state. Consequently, the magnetization of the top layer was reversed, and $M = 0$ was obtained by cooling the medium from T_{an} = 600 to 300 K, a temperature higher than T_{c1} = 526 K, T_{an}>T_{c1}. This process delivered a magnetic state of ↓↑ ("0"). For switching the bottom layer with high K_{bot} (2.7 ± 0.45 MJ/m^3), the reverse field was increased to $\mu_0 H = -1$ T, and the same process was followed. The magnetization of the bottom layer was reversed by cooling from 700 to 300 K, a temperature higher than T_{c2} = 610 K, T_{an}>T_{c2}. This delivered the magnetic state of ↓↓ ("−1″).

In addition, a multi-level HAMR recording simulation was performed based on the experimentally measured parameters. A heat spot with a Gaussian intensity distribution and a globally uniform write field of 0.2 T were used to heat the media and switch the magnetization in the desired direction as the media cooled down. Fig. 8 (a, b) shows images of the top and bottom layers at the end of a two-pass write process, as described in "Concept of multi-level recording in HAMR". Writing started with an AC-erased medium, corresponding to each grain being randomly magnetized either up or down. The first pass was written with T_{max} = 680 K, which was higher than the T_c of both layers, and a bit length of 50 nm. This resulted in the successful writing of both layers, but written track widths of ≈ 60 nm in the bottom layer and ≈ 100 nm in the top layer, owing to the different T_c ($T_{c1} < T_{c2}$). For the second pass, T_{max} was lowered to 540 K, which was below T_{c2}, to write only the top layer, and the bit length was increased to 100 nm. The bits were successfully written, but remnants of the first track remained at the track edges of the top layer, and the magnetization within the written bits was not fully saturated. This is attributed to the magnetization of some grains switching in opposite direction to the writing field during cooling. This problem can be solved by either increasing the write field or increasing K_u of the top layer. Fig. 8(c) shows the magnetization along the down-track direction in the top and bottom layers, averaged over a 40 nm track width, along with the sum of the magnetization of the two layers. Herein, four different magnetization states were observed. The magnetization corresponding to ↑↓ and ↓↑ was $M \neq 0$, and should allow 4-level recording as the anti-parallel states were easily distinguishable.

7. Conclusion

Proof of concept of multi-level recording has been successfully demonstrated for the first time by separating FePt-C (20 vol.%) nanogranular layers with a cubic Ru-C breaking layer. Both layers exhibited mainly a $L1_0$ ordered [001] texture along with certain in-plane variants based on micromagnetic simulation with a finite element model reproduced from experimental microstructural features. The higher variants in the top layer are attributed to the Ru diffusion and the spherical shape of FePt grains, resulting in a low $\mu_0 H_{c1}$ and K_{top} compared to the bottom layer. The T_c of each layer differed owing to Ru diffusion, deviations in the Fe and Pt content of the composition, and the order parameters, which facilitates multi-level recording.

The writing performance of the media was evaluated using experimental magnetic measurements and a HAMR recording simulation. Both layers were written successfully following the first pass; however, during the second pass, certain remnants of the first track remained in the top layer. This can be overcome by increasing K_{top} by improving the degree of the $L1_0$ order and by searching for a suitable spacer layer. After the two-pass writing, the magnetic states of ↑↑, ↓↓ were obtained, with ↑↓ and ↓↑ having M≠0, thus, allowing them to be distinguished and enabling an expansion from 3-level to 4-level recording. For this concept, due to the magnetic field strength of the magnetic head and the Curie temperature requirements, the number of layers is estimated to be three at most. Further optimization of microstructure and magnetic properties would pave the way to 10 Tbit/in^2.

Declaration of competing interest

The authors declare that they have no known competing financial interests or personal relationships that could have appeared to influence the work reported in this paper.

Acknowledgments

This work was supported in part by the JST-CREST (JPMJC22C3) and MEXT program: Data Creation and Utilization-Type Material Research and Development Project (JPMXP1122715503).

Supplementary materials

Supplementary material associated with this article can be found, in the online version, at doi:10.1016/j.actamat.2024.119869.

References

[1] D. Reinsel, J. Gantz, J. Rydning, The Digitization of the World from Edge to Core, 16, International Data Corporation, Framingham, 2018, pp. 1–26.
[2] V. Özdemir, N. Hekim, Birth of industry 5.0: Making sense of big data with artificial intelligence, "the internet of things" and next-generation technology policy, Omics J. Integr. Biol. 22 (2018) 65–76.
[3] G. Albuquerque, S. Hernandez, M.T. Kief, D. Mauri, L. Wang, HDD reader technology roadmap to an areal density of 4 tbpsi and beyond, IEEE Trans. on Magn. 58 (2021) 1–10.

[4] D. Weller, G. Parker, O. Mosendz, A. Lyberatos, D. Mitin, N.Y. Safonova, M. Albrecht, Review Article: FePt heat assisted magnetic recording media, J. Vac. Sci. Technol. B 34 (2016) 060801.

[5] X. Wang, K. Gao, H. Zhou, A. Itagi, M. Seigler, E. Gaga, HAMR recording limitations and extendibility, IEEE Trans. on Magn 49 (2013) 686–692.

[6] A.Q. Wu, Y. Kubota, T. Klemmer, T. Rausch, C. Peng, Y. Peng, D. Karns, X. Zhu, Y. Ding, E.K. Chang, Y. Zhao, HAMR areal density demonstration of 1+ Tbpsi on spinstand, IEEE Trans. on Magn. 49 (2013) 779–782.

[7] D. Weller, G. Parker, O. Mosendz, E. Champion, B. Stipe, X. Wang, T. Klemmer, G. Ju, A. Ajan, A HAMR media technology roadmap to an areal density of 4 Tb/in^2, IEEE Trans. on Magn. 50 (2013) 1–8.

[8] E. Roddick, M. Kief, A. Takeo, A new Advanced Storage Research Consortium HDD Technology Roadmap, in: IEEE 33rd Magnetic Recording Conference (TMRC), Milpitas, CA, USA, 2022, pp. 1–2, https://doi.org/10.1109/TMRC56419.2022.9918580.

[9] K. Hono, Y.K. Takahashi, G. Ju, J.U. Thiele, A. Ajan, X. Yang, R. Ruiz, L. Wan, Heat-assisted magnetic recording media materials, MRS Bull 43 (2018) 93–99.

[10] B.S.D. Varaprasad, Y.K. Takahashki, K. Hono, Microstructure control of $L1_0$-ordered FePt granular film for heat-assisted magnetic recording (HAMR) media, JOM 65 (2013) 853–861.

[11] D. Weller, O. Mosendz, G. Parker, S. Pisana, T.S. Santos, $L1_0$ FePtX–Y media for heat-assisted magnetic recording Phys, Status Solidi (a) 210 (2013) 1245–1260.

[12] P. Tozman, M. Venkatesan, L. Monzon, M. Coey, O. Kamer, Preparation of Fe-Pt powders from ingot by a simple and cost-effective spark erosion device, Cryst. Res. Technol. 57 (2022) 2200117.

[13] R.E. Rottmayer, S. Batra, D. Buechel, W.A. Challener, J. Hohlfeld, Y. Kubota, L. Li, B. Lu, C. Mihalcea, K. Mountfield, K. Pelhos, Heat-assisted magnetic recording, IEEE Trans. on Magn. 42 (2006) 2417–2421.

[14] I. Suzuki, J. Wang, Y.K. Takahashi, K. Hono, Control of grain density in FePt-C granular thin films during initial growth, J. Magn. Magn. Mater. 500 (2020) 166418.

[15] A. Bolyachkin, H. Sepehri-Amin, I. Suzuki, H. Tajiri, Y.K. Takahashi, K. Srinivasan, K. Ho, H. Yuan, T. Seki, A. Ajan, K. Hono, Transmission electron microscopy image based micromagnetic simulations for optimizing nanostructure of FePt-X heat-assisted magnetic recording media, Acta Mater 227 (2022) 117744.

[16] H. Pandey, J. Wang, T. Shiroyama, B.C.S. Varaprasad, H. Sepehri-Amin, Y. K. Takahashi, A. Perumal, K. Hono, Structure optimization of FePt–C nanogranular films for heat-assisted magnetic recording media, IEEE Trans. on Magn. 52 (2015) 1–8.

[17] L. Zhang, Y.K. Takahashi, A. Perumal, K. Hono, $L1_0$-ordered high coercivity (FePt) Ag–C granular thin films for perpendicular recording, J. Magn. Magn. Mater. 322 (2010) 2658–2664.

[18] Y.K. Takahashi, T. Koyama, M. Ohnuma, T. Ohkubo, K. Hono, Size dependence of ordering in FePt nanoparticles, J. Appl. Phys. 95 (2004) 2690–2696.

[19] B.S.D. Varaprasad, C. Xu, M.H. Huang, D.E. Laughlin, J.G. Zhu, FePt–BN granular HAMR media with high grain aspect ratio and high $L1_0$ ordering on corning LotusTM NXT glass, AIP Adv 13 (2023) 035002.

[20] C. Xu, B.S.D. Varaprasad, D.E. Laughlin, J.G. Zhu, Bias sputtering of granular L10-FePt films with hexagonal boron nitride grain boundaries, Sci. Rep. 13 (2023) 11087.

[21] C. Vogler, C. Abert, F. Bruckner, D. Suess, D. Praetorius, Heat-assisted magnetic recording of bit-patterned media beyond 10 Tb/in^2, Appl. Phys. Lett. 108 (2016) 102406.

[22] T.R. Albrecht, H. Arora, V. Ayanoor-Vitikkate, J.M. Beaujour, D. Bedau, D. Berman, A.L. Bogdanov, Y.A. Chapuis, J. Cushen, E.E. Dobisz, G. Doerk, Bit-patterned magnetic recording: Theory, media fabrication, and recording performance, IEEE Trans. on Magn. 51 (2015) 1–42.

[23] M. Albrecht, G. Hu, A. Moser, O. Hellwig, B.D. Terris, Magnetic dot arrays with multiple storage layers, J. Appl. Phys. 97 (2005) 103910.

[24] H. Suto, T. Nagasawa, K. Kudo, T. Kanao, K. Mizushima, R. Sato, Layer-selective switching of a double-layer perpendicular magnetic nanodot using microwave assistance, Phys. Rev. Appl. 5 (2016) 014003.

[25] G. Winkler, D. Suess, J. Lee, J. Fidler, M.A. Bashir, J. Dean, A. Goncharov, G. Hrkac, S. Bance, T, Schrefl Microwave-assisted three-dimensional multilayer magnetic recording, Appl. Phys. Lett. 94 (2009) 232501.

[26] S.J. Greaves, K.S. ChanY. Kanai, Areal density capability of dual-structure media for microwave-assisted magnetic recording, IEEE Trans. on Magn. 55 (2019) 1–9.

[27] T. Kobayashi, Y. Nakatani, Y. Fujiwara, Media design for three-dimensional heat-assisted magnetic recording, J. Magn Soc. Jpn. 44 (2020) 122–128.

[28] T. Kobayashi, Y. Nakatani, Y. Fujiwara, Information stability in three-dimensional heat-assisted magnetic recording, J. Magn Soc. Jpn. 44 (2020) 34–39.

[29] V.V. Mehta, J.W. Reiner, M.P. Salo, R.W. Wood, Heat-assisted magnetic recording (HAMR) disk drive with disk having multiple continuous magnetic recording layers, U.S. Patent No: 9 (2017) 144, 601.

[30] J.-G. Zhu, Y. Yan, Incoherent Magnetic Switching of $L1_0$ FePt Grains, IEEE Trans. on Magn. 57 (2021) 1–9.

[31] T.Y. Chang, P. Steiner, A. Venugopal, J. Jury, P.W. Huang, A. Ghoreyshi, S. Hernandez, Zero-state insert dual layer HAMR media recording, IEEE Trans. on Magn. 59 (2022) 3200107.

[32] J. Park, Y.K. Hong, S.G. Kim, L. Gao, J.U. Thiele, Magnetic properties of Fe-Mn-Pt for heat assisted magnetic recording applications, J. Appl. Phys. 117 (2015) 053911.

[33] T. Ono, H. Nakata, T. Moriya, S.Okamoto N.Kikuchi, O. Kitakami, T. Shimatsu, Experimental investigation of off-stoichiometry and 3d transition metal (Mn, Ni, Cu)-substitution in single-crystalline FePt thin films, AIP Adv 6 (2016) 056011.

[34] S.D. Granz, K. Barmak, M.H. Kryder, Granular $L1_0$ FePt-B and FePt-B-Ag (001) thin films for heat assisted magnetic recording, J. Appl. Phys. 111 (2012) 07B709.

[35] Y. Kota, First-principles calculation of Curie temperature tuning in $L1_0$-type FePt by element substitution of Mn, Cu, Ru, and Rh, J. Magn Soc. Jpn. 44 (2020) 1–4.

[36] J. Wang, S. Hata, Y.K. Takahashi, H. Sepehri-Amin, B.S.D. Varaprasad, T. Shiroyama, T. Schrefl, K. Hono, Effect of MgO underlayer misorientation on the texture and magnetic property of FePt–C granular film, Acta Mater 91 (2015) 41–49.

[37] M.D. Kuz'min, D M, Shape of temperature dependence of spontaneous magnetization of ferromagnets: quantitative analysis, Phys. Rev. Lett. 94 (2005) 107204.

[38] T. Ono, N. Kikuchi, S. Okamoto, O. Kitakami, T. Shimatsu, Novel torque magnetometry for uniaxial anisotropy constants of thin films and its application to FePt granular thin films, Appl. Phys. Exp. 11 (2018) 033002.

[39] J. Wang, H. Sepehri-Amin, T.Nakamura H.Tajiri, K. Masuda, Y.K. Takahashi, T. Ina, T. Uruga, I. Suzuki, Y. Miura, K. Hono, Impact of carbon segregant on microstructure and magnetic properties of FePt-C nanogranular films on MgO (001) substrate, Acta Mater 166 (2019) 413–423.

[40] R. Chang, S. Li, M.V. Lubarda, B. Livshitz, V. Lomakin, FastMag: Fast micromagnetic simulator for complex magnetic structures, J. Appl. Phys. 109 (2011) 07D358.

[41] R.F.L. Evans, D. Hinzke, U. Atxitia, U. Nowak, R.W. Chantrell, O. Chubykalo-Fesenko, Stochastic form of the Landau-Lifshitz-Bloch equation, Phys. Rev. B 85 (2012) 014433.

[42] S.J. Greaves, H. Muraoka, Y. Kanai, Modelling of thermally assisted magnetic recording with the LLB equation and Brillouin functions, J. Appl. Phys. 117 (2015) 17C505.

[43] D.L. Zhang, C. Sun, Y. Lv, K.B. Schliep, Z. Zhao, J.Y. Chen, P.M. Voyles, J.P. Wang, L10 FePd synthetic antiferromagnet through an fcc Ru spacer utilized for perpendicular magnetic tunnel junctions, Phys. Rev. Appl. 9 (2018) 044028.

[44] T. Ono, H. Nakata, T. Moriya, N. Kikuchi, S. Okamoto, O. Kitakami, T. Shimatsu, Addition of Ru to $L1_0$-FePt thin film to lower Curie temperature, Appl. Phys. Express. 9 (2016) 123002.

[45] S. Okamoto, N. Kikuchi, O. Kitakami, T. Miyazaki, Y. Shimada, K. Fukamichi, Chemical-order-dependent magnetic anisotropy and exchange stiffness constant of FePt (001) epitaxial films, Phys. Rev. B 66 (2002) 024413.

[46] M. Watanabe, T. Masumoto, Extraordinary Hall effect in Fe–Pt alloy thin films and fabrication of micro Hall devices, Thin Solid Films 405 (2002) 92–97.

[47] A. Perumal, H.S. Ko, S.C. Shin, Perpendicular thin films of carbon-doped FePt for ultrahigh-density magnetic recording media, IEEE Trans. on Magn. 39 (2003) 2320–2322.

[48] C. Feng, J. Zhao, F. Yang, K. Gong, S.:. Hao, Y. Cao, C. Hu, J. Zhang, Z. Wang, L. Chen, S. Li, Nonvolatile modulation of electronic structure and correlative magnetism of $L1_0$-FePt films using significant strain induced by shape memory substrates, Sci. Rep. 6 (2016) 1–10.